# Surface magnetism in pristine α rhombohedral boron and intersurface exchange coupling mechanism of boron icosahedra

Xiao Yu, Tiege Zhou, Yuanchun Zhao, Feng Lu, Xiaoming Zhang, Guodong Liu, Huiyang Gou, Eva Zurek, and Xiaoguang Luo\*

ABSTRACT: We report intrinsic surface magnetism in pristine  $\alpha$  rhombohedral boron ( $\alpha$ -boron) using first-principles calculations. Semiconducting  $\alpha$ -boron has been cleaved along (001), (10-2), and (101) planes to produce icosahedral-based non-van der Waals face-boron, t-face-boron and edge-boron structures, respectively. Face-boron is found to be metallic, while t-face-boron and edge-boron show semiconducting features. In particular, edge-boron exhibits layer-dependent magnetism with a transition from an overall antiferromagnetic (AFM) state with AFM surfaces to either an AFM or ferromagnetic (FM) state with FM surfaces as the number of layers increases. The magnetism in edge-boron arises from the spin polarization of boron atoms with unsaturated bonds at the edge sites in the upper and lower surfaces, and magnetic exchange coupling can be mediated via adjacent boron icosahedra by up to a maximum of 8.4 Å. These findings deepen our understanding of icosahedral-based boron and boron-rich materials, which may be useful in potential spintronics applications.

Ever since graphene was mechanically exfoliated from graphite, various two-dimensional (2D) materials such as silicene, <sup>2</sup> GeH, <sup>3</sup> MoS<sub>2</sub>, <sup>4</sup> and borophene, <sup>5-7</sup> each with their own distinctive attractive physical properties, have been synthesized. Boron is a unique element due to its ability to adopt a wide variety of multicenter bonding schemes leading to structural diversity in the clusters, sheets, and extended structures it may assume.<sup>8-11</sup> A series of 2D boron materials including monolaver, buckled double layer, and multilayer borophenes have been reported, exhibiting metallic, semiconducting, Dirac-related, and magnetic properties. 12-29 Another way to construct quasi-2D boron lattices is based on boron icosahedra, 30-31 because they are a common structural motif presents in three-dimensional (3D) boron lattices of  $\alpha$  rhombohedral boron ( $\alpha$ -boron), <sup>32</sup>  $\beta$  rhombohedral boron ( $\beta$ -boron), <sup>33</sup> and  $\gamma$ boron.<sup>34</sup> Theoretical investigations have shown a layer of boron icosahedra is not stable on Cu and Ni, but stable on Au and Ag substrates. 12 The surface energy of  $\alpha$ -boron and  $\beta$ -boron have been investigated, 35 and the surface reconstructions of the  $\alpha$ -boron (111) plane have also been studied. 36-37 Traditional magnetic materials are generally composed of metallic elements with d- or f-electrons and their magnetic properties are governed by magnetic exchange interactions. Many exchange coupling mechanisms, e.g., direct exchange, double exchange, super exchange, and Ruderman-Kittel-Kasuya-Yosida (RKKY) interactions,<sup>38</sup> have been established to explain the classical magnetism arising from d- or f-electrons. After the discovery of 2D magnetism in the van der Waals solid CrI<sub>3</sub>,<sup>39</sup> a Bethe-Slater-curve (BSC)-like behavior in 2D transition metal dichalcogenide bilayers was reported and explained by the extended superexchange mechanism. <sup>40</sup> The BSC was originally used to describe magnetic ordering in 3d metallic elements.<sup>41</sup> Recently, the origin of magnetism in light-element materials containing s- and p-electrons only has attracted great interest. For example, magnetism has been reported in boron<sup>24-28</sup> and carbon<sup>42-51</sup> allotropes with low-dimensional structures. A recently claimed 3D carbon allotrope (dubbed U-carbon) is an exciting example of a bulk light-element magnetic material.<sup>52</sup> However, currently it remains unclear if the traditional mechanisms are applicable in light-element systems.

In this work, first-principles calculations investigating icosahedral-based 2D boron allotropes unveil their potential for surface magnetism, and an exchange coupling mechanism explaining this behavior is proposed. We show that the semiconducting bulk  $\alpha$ -boron can have metallic, semiconducting, and magnetic surfaces. The layer-dependent surface magnetism in pristine  $\alpha$ -boron is explained by an exchange coupling mechanism of boron icosahedra. The magnetism arises from the spin polarization of boron atoms with unsaturated bonds at the outermost parts in the upper and lower surfaces of specific arrangements of boron icosahedra, and magnetic exchange coupling between them ultimately determine the surface magnetism of  $\alpha$ -boron. The mechanism, based on s- and p-electrons, differs from the traditional exchange coupling mechanisms based on d- or f-electrons, and it is generally to be applied to light-element magnetic materials, especially icosahedral-based boron and boron-rich materials.

Density functional theory calculations were performed using the Vienna Ab-initio Simulation Package (VASP)<sup>53</sup> with the projector-augmented wave method (PAW) method<sup>54</sup>, and the Perdew-Burke-Ernzerhof (PBE)<sup>55</sup> functional within the generalized gradient approximation (GGA)<sup>56</sup>. An energy cut-off of 600 eV was selected and Monkhorst-Pack meshes<sup>57</sup> with a reciprocal space resolution of  $2\pi \times 0.02$  Å<sup>-1</sup> were used. A vacuum slab of 15 Å was employed for all non-van der Waals few-layer structures. The structural relaxation parameters were set to  $10^{-6}$  eV and 0.01 eV/Å. Non-spherical contributions from the gradient corrections inside the PAW spheres were used. The phonon spectra were calculated using phonopy with the finite-displacement approach.<sup>58</sup> Solid-state adaptive

natural density partitioning (SSAdNDP)<sup>59-61</sup> with 6-31G\* basis set was used to analyze the chemical bonding of cleaved layer structures.

In this work  $\alpha$ -boron in a hexagonal representation is used to construct quasi-2D structures composed entirely of boron icosahedra. The boron icosahedron is taken as a crystal motif in the unit cell of  $\alpha$ -boron, which possesses ABCABC... stacking sequences along the [001] direction, as shown in Figure 1a. Here we propose two rules to produce icosahedral-based single-layer structures. First, each icosahedron must be protected from being broken during the cleaving process. Second, neighboring icosahedra should be directly connected to each other to avoid structural fragmentation. Only three possible cleavage planes of (001), (10-2), and (101), as shown in Figure 1a, satisfy the above rules, and the obtained single-layers are named as face-boron, t-face-boron, and edge-boron (Figure 1b-d), respectively. From this point of view,  $\alpha$ -boron can be considered as ABCABC... stacking along the (101) plane or ABAB... stacking along the (10-2) plane, in addition to the already known ABCABC... stacking along the (001) plane.

Both the unit cells of face-boron and t-face-boron, as well as the primitive cell of edge-boron, consist of one boron icosahedron. The locations of the outermost atoms at the upper and lower surfaces of these three structures as depicted in red, blue, and pink in Figure 1b-d, are named as face sites, t-face sites, and edge sites, respectively. Other locations besides the aforementioned outermost sites are inner sites. The face and inner sites in face-boron correspond to the polar and equatorial sites of bulk  $\alpha$ -boron, respectively. As for the edge-boron structure, the atoms at the edge sites form edge-shaped B-B bonds, which are parallel to the basal plane and in a mirror-distributed manner (Figure 1d). In comparison with twelve surrounding boron icosahedra with six 3c-2e bonds and six 2c-2e bonds in  $\alpha$ -boron, the icosahedra in face-boron are surrounded by six icosahedra with six 3c-2e bonds.

The icosahedra in t-face-boron and edge-boron are surrounded by four and six icosahedra with six and eight 2c-2e bonds, respectively. In all these structures, geometrical relaxation shrinks the intericosahedral B-B bonds corresponding to the 3c-2e bonds in  $\alpha$ -boron, while those originating from the 2c-2e bonds exhibit an increase. The total energies of these three single-layer structures are found to be  $E_{\text{edge-boron}} < E_{\text{t-face-boron}} < E_{\text{face-boron}}$  (Table S1), and this trend is the same as that of the corresponding surface energies.<sup>35</sup>

The electronic band structure in a fat-band representation and local density of states (LDOS) of face-boron indicates metallic features as shown in Figure 2a. The contributions to the two energy bands crossing the Fermi level are primarily from the face sites, suggesting that the unsaturated bonds on the surface are the main reason for the metallicity. An indirect band gap of 0.11 eV is found in t-face-boron (Figure 2b), with the valence band maximum (VBM) located at the  $\Gamma$  point and the conduction band minimum (CBM) at the C point. The VBM contains almost equal contributions from the t-face and inner sites, while the two conduction bands closest to the Fermi level are primarily due to contributions from the t-face sites. Edge-boron is also found to be a semiconductor but with a direct band gap of 0.19 eV located at the  $\Gamma$  point (Figure 2c), and the energy bands closest to the Fermi level are mainly composed of contributions from the edge sites.

With respect to the three single-layer structures shown in Figure 1b-d, spin-polarized relaxations reveal that only edge-boron is magnetic. As listed in Table S2, two AFM configurations, AFM-4 ( $\uparrow\downarrow\uparrow\downarrow\downarrow\uparrow\uparrow$ ) and AFM-5 ( $\downarrow\uparrow\uparrow\downarrow\uparrow\downarrow\uparrow\uparrow$ ), have been found after relaxation. The spin-polarized band structure and density of states (DOS) of AFM-4 and AFM-5 edge-boron are shown in Figure 3a and Figure S1, respectively. Both of them possess an indirect band gap with the CBM and VBM located between the  $\Gamma$  and Y points, in contrast to the direct band gap observed in the NM (non-magnetic)

state (Figure 2c). The calculated band gap is 0.64 eV for AFM-4 and 0.38 eV for AFM-5, respectively. The spin-polarized band structure in a fat-band representation of AFM-4 edge-boron further indicates that the edge sites contribute more to the energy band around the VBM than the inner sites, and these two sites almost equally contribute to the energy band around the CBM (Figure S2). The spin-polarized LDOS of the edge sites in AFM-4 and AFM-5 (Figure S3) illustrate that the spin-up state is different from the spin-down state, confirming their AFM characteristics. All of the boron atoms at edge sites in AFM-4 and AFM-5 possess a uniform absolute value of the local magnetic moment of  $0.18 \mu\text{B}$ , while the local magnetic moment of the atoms in the inner sites are zero. The calculated spin-polarized total energies of edge-boron show the following order of stability:  $E_{\text{AFM-4}} < E_{\text{AFM-5}} < E_{\text{NM}}$ , as summarized in Table S1. The phonon band structure of spin-polarized AFM-4 edge-boron indicates that it is dynamically stable (Figure S4). The local magnetic moments of antiparallel arrangement are evident in the spin-polarized charge density of AFM-4 edge-boron shown in Figure 3b. Therefore, the ground state of single-layer edge-boron should be in an AFM state with AFM surfaces.

As far as 2-layer edge-boron is concerned, our electronic structure calculations show that an AFM-1 configuration is the ground state among five possible configurations (Table S2). The spin-polarized band structure, DOS, and charge density of 2-layer AFM-1 edge-boron are displayed in Figure 3c-d, and those of the other magnetic configurations are shown in Figure S5. Figure 3c illustrates that 2-layer AFM-1 edge-boron possesses an indirect band gap of 0.52 eV with both the VBM and CBM located between the  $\Gamma$  and Y points. The LDOS of the boron atoms at the edge sites (Figure S6) confirms its AFM state, and Figure 3d shows the localization of spin density in the upper and lower surfaces with opposite spin directions. Therefore, the ground state of 2-layer edge-boron is predicted

to be AFM with FM surfaces. The boron atoms at the edge sites in this structure have one of two magnetic moments with absolute values of 0.15 and  $0.24 \,\mu\text{B}$ , while the boron atoms at the inner sites possess non-zero local magnetic moments that are  $1\sim2$  orders of magnitude smaller than those of the edge sites.

Figure 4a shows how the calculated GGA-PBE band gap of the non-van der Waals few-layer structure depends on the number of layers (n). As n increases, face-boron (t-face-boron) retains its metallic (semiconducting) features (Figure S7-8). Although the single-layer NM edge-boron possesses an indirect band gap of 0.19 eV, the corresponding 2~6 layer structures show similar features to face-boron (Figure S9). However, the spin-polarized calculations reveal unexpected semiconducting features of the multilayer ground-state of edge-boron (Figure 4a), and the obtained band gaps exhibit a three-stage variation with respect to n (Figure S10-17). The first stage, with an indirect band gap of 0.64 eV, corresponds to an AFM ground state with AFM upper/lower surfaces for 1-layer. The second stage, for 2~4-layer structures, corresponds to an AFM ground state with FM surfaces with an indirect band gap of 0.52~0.53 eV. In the third stage, observed in 5~6-layer structures, the indirect band gap further decreases to 0.48~0.42 eV corresponding to AFM or FM ground states with FM surfaces. The decreased band gap is mainly a result of a change of the energy level of the VBM, which is accompanied with a change in the location from the  $\Gamma$ -Y high symmetry line to the  $\Gamma$ point. The VBM of the FM-1 and AFM-1 configurations mainly contain contributions from the inner sites, similar to what was observed in the 4~6-layer t-face-boron (Figure S8). Figure 4b shows the relationship of the energy difference  $(E_d)$  of various edge-boron configurations with respect to the corresponding NM states as a function of n, indicating the total energy of spin-polarized states are remarkably lower for all of the structures considered. As n increases, the determined  $E_d$  gradually

increases and then converges to about -0.75 eV per unit cell.

Figure 4c shows the layer dependent energy difference between the most stable AFM and FM configurations of edge-boron. As n increases, the energy difference gradually decreases and converges to nearly zero for  $n \ge 3$ , which differs from the interlayer distance-dependent AFM to FM transition with BSC-like behavior as observed in 2D CrSe<sub>2</sub> bilayers, <sup>40</sup> as well as the oscillating interlayer AFM/FM behavior in RKKY interactions.<sup>38</sup> This indicates that the extended superexchange and RKKY mechanisms cannot describe the surface magnetism in edge-boron systems that do not contain d- and f-electrons. The surface magnetism of edge-boron is rather produced from s- and pelectrons only, whose wave functions and associated electron densities differ from those of d- and felectrons. Moreover, note that the traditional mechanisms have been developed mainly for elements and compounds with 2c-2e bonds, while edge-boron also contains multicenter bonds. Therefore, we propose an exchange coupling interaction mechanism to explain the calculated results based on boron icosahedra. The magnetism in edge-boron arises from the spin-polarization of the boron atoms with unsaturated bonds at the surface edge sites. It can be divided into three parts: the intrasurface magnetism from the exchange coupling between the boron atoms at the edge sites inside each icosahedron (XC<sub>intra-i</sub>, e.g. atoms B5 and B6 in Figure 1d) and those between the intrasurface icosahedra (XC<sub>intra-b</sub>, e.g. atoms B6 and B7 in Figure 1d), and the intersurface magnetism from the exchange coupling (XC<sub>inter</sub>) between the upper and lower surfaces. As n increases, the XC<sub>intra-i</sub> and  $XC_{intra-b}$  remain essentially constant due to the small changes in the a and b lattice constants (less than 0.13 Å), while XC<sub>inter</sub> is strongly dependent on the layer spacing. XC<sub>intra-i</sub> has the strongest coupling because of the smallest distance (1.60~1.63 Å) between the edge sites at the surface. The distance between the intersurface B2-B5 (3.15 Å) and B2-B6 (2.70 Å) atoms in 1-layer AFM-4 configuration

is smaller than that of intrasurface B2-B3 (3.72 Å) (Figure 1d), and thus XC<sub>inter</sub> is larger than the corresponding XC<sub>intra-b</sub>. The strong XC<sub>inter</sub> is responsible for the AFM surfaces with uniform local magnetic moments of 0.18 µB at the edge sites and zero local magnetic moments at the inner sites. For an extended spacing of 6.75 Å in 2-layer AFM-1 configuration, the distance between the nearest neighboring edge sites, 3.76 Å, is less than the minimum distance between the edge sites at the upper and lower surfaces (6.90 Å). As a result, the strength of XC<sub>intra-b</sub> is larger than that of XC<sub>inter</sub>, and the two different local magnetic moments of 0.15 and 0.24 µB at the edge sites mainly result from XC<sub>intra-</sub> i and XC<sub>intra-b</sub>. The small but non-zero local magnetic moments at the inner sites indicate that the exchange coupling range of XC<sub>inter</sub> is at least 6.90 Å. For larger spacings, the strength of the XC<sub>inter</sub> in 3-layer AFM-1 edge-boron is close to zero, and those of 4~6 layered configurations are found to be zero at the level of accuracy of our DFT calculations. The maximum distance of XC<sub>inter</sub> of 8.4 Å can be inferred from the non-zero local magnetic moments in 3-layer AFM-1 edge-boron, indicating that the local magnetic moments at the edge sites are mainly affected by the six intrasurface neighboring boron icosahedra because the calculated magnetic anisotropy is almost zero within the accuracy of the calculation method. Configurations of 4~6-layer edge-boron show either FM or AFM features with FM surfaces because only XC<sub>intra-i</sub> and XC<sub>intra-b</sub> are responsible for the upper or lower surfaces, which indeed produce two local magnetic moments with absolute values of 0.14 and 0.27 μB for the boron atoms at the edge sites.

In summary, we theoretically predict the surface magnetism in pristine  $\alpha$ -boron by inspecting specific icosahedral-based layer structures, and propose an exchange coupling mechanism to explain the magnetic behavior. Among three types of structures considered, only the so-called "edge-boron" structure with edge-shaped B-B bonds at the outermost surfaces exhibits magnetism, which arises

from the spin-polarization of the boron atoms at the edge sites with unsaturated bonds in the upper and lower surfaces. The ground state of 1-layer edge-boron possesses an AFM state with AFM upper/lower surfaces, and the 2-layer edge-boron has an AFM state with FM surfaces. For multilayer structures (5 layers and more), their ground states could be AFM or FM with FM surfaces, suggesting that bulk α-boron has FM surfaces. The layer-dependent surface magnetism, with a transition from AFM to AFM/FM, is explained by the exchange coupling mechanism between the spin-polarized boron atoms within or crossing the icosahedral motifs. The maximum distance of magnetic exchange coupling is 8.4 Å in edge-boron. This work presents an insight into the unique surface magnetism induced by specific icosahedral-based configurations in pure boron, providing new opportunities for the design and engineering of future spintronic devices.

## ASSOCIATED CONTENT

**Supporting Information.** This material is available free of charge via the Internet at http://pubs.acs.org.

Phonon stability, ground state checking, discussions of face-boron and t-face-boron, supplementary tables (S1-S2), and supplementary figures (S1-S17).

#### **AUTHOR INFORMATION**

# **Corresponding Author**

**Xiaoguang Luo** - Department of Electronics, College of Electronic Information and Optical Engineering, Nankai University, Tianjin 300071, China; Email: luoxg@nankai.edu.cn

## **Authors**

**Xiao Yu** - School of Materials Science and Engineering, Hebei University of Technology, Tianjin 300130, China

**Tiege Zhou** - Department of Electronics, College of Electronic Information and Optical Engineering, Nankai University, Tianjin 300071, China

**Yuanchun Zhao** - State Key Laboratory of Metastable Materials Science and Technology, Yanshan University, Qinhuangdao 066004, China

**Feng Lu** - Department of Electronics, College of Electronic Information and Optical Engineering, Nankai University, Tianjin 300071, China

**Xiaoming Zhang** - School of Materials Science and Engineering, Hebei University of Technology, Tianjin 300130, China

**Guodong Liu** - School of Materials Science and Engineering, Hebei University of Technology, Tianjin 300130, China

**Huiyang Gou** - Center for High Pressure Science and Technology Advanced Research, Beijing 100094, China

**Eva Zurek** - Department of Chemistry, State University of New York at Buffalo, Buffalo, New York 14260, United States

#### Notes

The authors declare no competing financial interest.

#### **ACKNOWLEDGMENTS**

Y.C.Z. acknowledges the National Natural Science Foundation of China (grants no. 51772261 and

52072332). E.Z. acknowledges the NSF (DMR-1827815) for financial support.

## REFERENCES

- (1) Novoselov, K. S.; Geim, A. K.; Morozov, S. V.; Jiang, D.; Zhang, Y.; Dubonos, S. V.; Grigorieva, I. V.; Firsov, A. A., Electric field effect in atomically thin carbon films. *Science* **2004**, *306* (5696), 666-669.
- (2) Vogt, P.; De Padova, P.; Quaresima, C.; Avila, J.; Frantzeskakis, E.; Asensio, M. C.; Resta, A.; Ealet, B.; Le Lay, G., Silicene: Compelling experimental evidence for graphenelike two-dimensional silicon. *Phys. Rev. Lett.* **2012**, *108* (15), 155501.
- (3) Bianco, E.; Butler, S.; Jiang, S. S.; Restrepo, O. D.; Windl, W.; Goldberger, J. E., Stability and exfoliation of germanane: A germanium graphane analogue. *ACS Nano* **2013**, *7* (5), 4414-4421.
- (4) Mak, K. F.; Lee, C.; Hone, J.; Shan, J.; Heinz, T. F., Atomically thin MoS<sub>2</sub>: A new direct-gap semiconductor. *Phys. Rev. Lett.* **2010**, *105* (13), 136805.
- (5) Mannix, A. J.; Zhou, X. F.; Kiraly, B.; Wood, J. D.; Alducin, D.; Myers, B. D.; Liu, X. L.; Fisher, B. L.; Santiago, U.; Guest, J. R.; Yacaman, M. J.; Ponce, A.; Oganov, A. R.; Hersam, M. C.; Guisinger, N. P., Synthesis of borophenes: Anisotropic, two-dimensional boron polymorphs. *Science* **2015**, *350* (6267), 1513-1516.
- (6) Feng, B. J.; Zhang, J.; Zhong, Q.; Li, W. B.; Li, S.; Li, H.; Cheng, P.; Meng, S.; Chen, L.; Wu, K. H., Experimental realization of two-dimensional boron sheets. *Nature Chem.* **2016**, *8* (6), 564-569.
- (7) Wu, R. T.; Drozdov, I. K.; Eltinge, S.; Zahl, P.; Ismail-Beigi, S.; Bozovic, I.; Gozar, A., Largearea single-crystal sheets of borophene on Cu(111) surfaces. *Nature Nanotech.* **2019**, *14* (1), 44-50.
- (8) He, J. L.; Wu, E. D.; Wang, H. T.; Liu, R. P.; Tian, Y. J., Ionicities of boron-boron bonds in B<sub>12</sub> icosahedra. *Phys. Rev. Lett.* **2005**, *94* (1), 015504.

- (9) Kunstmann, J., Modeling sp materials: Novel phases of elemental boron, structure control of nanotubes, and the enatom method. Südwestdeutscher Verlag für Hochschulschriften: Saarbrücken, 2009.
- (10) Sun, X.; Liu, X. F.; Yin, J.; Yu, J.; Li, Y.; Hang, Y.; Zhou, X. C.; Yu, M. L.; Li, J. D.; Tai, G. A.; Guo, W. L., Two-dimensional boron crystals: Structural stability, tunable properties, fabrications and applications. *Adv. Func. Mater.* **2017**, *27* (19), 1603300.
- (11) Saha, S.; Linden, W. v. d.; Boeri, L., Fused borophenes: A new family of superhard materials. *arXiv* **2021**, 2101.10013.
- (12) Zhang, Z. H.; Yang, Y.; Gao, G. Y.; Yakobson, B. I., Two-dimensional boron monolayers mediated by metal substrates. *Angew. Chem. Int. Ed.* **2015**, *54* (44), 13022-13026.
- (13) Penev, E. S.; Bhowmick, S.; Sadrzadeh, A.; Yakobson, B. I., Polymorphism of two-dimensional boron. *Nano Lett.* **2012**, *12* (5), 2441-2445.
- (14) Yu, X.; Li, L. L.; Xu, X. W.; Tang, C. C., Prediction of two-dimensional boron sheets by particle swarm optimization algorithm. *J. Phys. Chem. C* **2012**, *116* (37), 20075-20079.
- (15) Xu, S. G.; Li, X. T.; Zhao, Y. J.; Liao, J. H.; Xu, W. P.; Yang, X. B.; Xu, H., Two-dimensional semiconducting boron monolayers. *J. Am. Chem. Soc.* **2017**, *139* (48), 17233-17236.
- (16) Zhang, H. H.; Xie, Y.; Zhang, Z. W.; Zhong, C. Y.; Li, Y. F.; Chen, Z. F.; Chen, Y. P., Dirac nodal lines and tilted semi-Dirac cones coexisting in a striped boron sheet. *J. Phys. Chem. Lett.* **2017**, 8 (8), 1707-1713.
- (17) Yi, W. C.; Liu, W.; Botana, J.; Zhao, L.; Liu, Z.; Liu, J. Y.; Miao, M. S., Honeycomb boron allotropes with Dirac cones: A true analogue to graphene. *J. Phys. Chem. Lett.* **2017**, *8* (12), 2647-2653.

- (18) Ezawa, M., Triplet fermions and Dirac fermions in borophene. *Phys. Rev. B* **2017**, *96* (3), 035425.
- (19) Feng, B. J.; Sugino, O.; Liu, R. Y.; Zhang, J.; Yukawa, R.; Kawamura, M.; Iimori, T.; Kim, H.; Hasegawa, Y.; Li, H.; Chen, L.; Wu, K. H.; Kumigashira, H.; Komori, F.; Chiang, T. C.; Meng, S.; Matsuda, I., Dirac fermions in borophene. *Phys. Rev. Lett.* **2017**, *118* (9), 096401.
- (20) Tang, H.; Ismail-Beigi, S., Novel precursors for boron nanotubes: The competition of two-center and three-center bonding in boron sheets. *Phys. Rev. Lett.* **2007**, *99* (11), 115501.
- (21) Zhou, X. F.; Dong, X.; Oganov, A. R.; Zhu, Q.; Tian, Y. J.; Wang, H. T., Semimetallic two-dimensional boron allotrope with massless Dirac fermions. *Phys. Rev. Lett.* **2014**, *112* (8), 085502.
- (22) Ma, F. X.; Jiao, Y. L.; Gao, G. P.; Gu, Y. T.; Bilic, A.; Chen, Z. F.; Du, A. J., Graphene-like two-dimensional ionic boron with double Dirac cones at ambient condition. *Nano Lett.* **2016**, *16* (5), 3022-3028.
- (23) Xu, S. G.; Zheng, B. B.; Xu, H.; Yang, X. B., Ideal nodal line semimetal in a two-dimensional boron bilayer. *J. Phys. Chem. C* **2019**, *123* (8), 4977-4983.
- (24) Zhou, X. F.; Oganov, A. R.; Wang, Z. H.; Popov, I. A.; Boldyrev, A. I.; Wang, H. T., Two-dimensional magnetic boron. *Phys. Rev. B* **2016**, *93* (8), 085406.
- (25) Zhu, M. H.; Weng, X. J.; Gao, G.; Dong, S.; Lin, L. F.; Wang, W. H.; Zhu, Q.; Oganov, A. R.; Dong, X.; Tian, Y. J.; Zhou, X. F.; Wang, H. T., Magnetic borophenes from an evolutionary search. *Phys. Rev. B* **2019**, *99* (20), 205412.
- (26) Tkachenko, N. V.; Steglenko, D.; Fedik, N.; Boldyreva, N. M.; Minyaev, R. M.; Minkin, V. I.; Boldyrev, A. I., Superoctahedral two-dimensional metallic boron with peculiar magnetic properties. *Phys. Chem. Chem. Phys.* **2019**, *21* (36), 19764-19771.

- (27) Vishkayi, S. I.; Tagani, M. B., Edge-dependent electronic and magnetic characteristics of freestanding β<sub>12</sub>-borophene nanoribbons. *Nano-Micro Lett.* **2018**, *10* (1), 14.
- (28) Vishkayi, S. I.; Tagani, M. B., Freestanding χ<sub>3</sub>-borophene nanoribbons: A density functional theory investigation. *Phys. Chem. Chem. Phys.* **2018**, *20* (15), 10493-10501.
- (29) Tsai, H. S.; Hsiao, C. H.; Lin, Y. P.; Chen, C. W.; Ouyang, H.; Liang, J. H., Fabrication of multilayer borophene on insulator structure. *Small* **2016**, *12* (38), 5251-5255.
- (30) Lau, K. C.; Pandey, R., Stability and electronic properties of atomistically-engineered 2D boron sheets. *J. Phys. Chem. C* **2007**, *111* (7), 2906-2912.
- (31) Kah, C. B.; Yu, M.; Tandy, P.; Jayanthi, C. S.; Wu, S. Y., Low-dimensional boron structures based on icosahedron B<sub>12</sub>. *Nanotech.* **2015**, *26* (40), 405701.
- (32) Albert, B.; Hillebrecht, H., Boron: Elementary challenge for experimenters and theoreticians. *Angew. Chem. Int. Ed.* **2009**, *48* (46), 8640-8668.
- (33) Ogitsu, T.; Gygi, F.; Reed, J.; Motome, Y.; Schwegler, E.; Galli, G., Imperfect crystal and unusual semiconductor: Boron, a frustrated element. *J. Am. Chem. Soc.* **2009**, *131* (5), 1903-1909.
- (34) Oganov, A. R.; Chen, J. H.; Gatti, C.; Ma, Y. Z.; Ma, Y. M.; Glass, C. W.; Liu, Z. X.; Yu, T.; Kurakevych, O. O.; Solozhenko, V. L., Ionic high-pressure form of elemental boron. *Nature* **2009**, 457 (7231), 863-867.
- (35) Hayami, W.; Otani, S., The role of surface energy in the growth of boron crystals. *J. Phys. Chem. C* **2007**, *111* (2), 688-692.
- (36) Amsler, M.; Botti, S.; Marques, M. A. L.; Goedecker, S., Conducting boron sheets formed by the reconstruction of the α-boron (111) surface. *Phys. Rev. Lett.* **2013**, *111* (13), 136101.
- (37) Zhou, X. F.; Oganov, A. R.; Shao, X.; Zhu, Q.; Wang, H. T., Unexpected reconstruction of the

- α-boron (111) surface. Phys. Rev. Lett. 2014, 113 (17), 176101.
- (38) Parkin, S. S. P.; More, N.; Roche, K. P., Oscillations in exchange coupling and magnetoresistance in metallic superlattice structures: Co/Ru, Co/Cr, and Fe/Cr. *Phys. Rev. Lett.* **1990**, 64 (19), 2304-2307.
- (39) Huang, B.; Clark, G.; Navarro-Moratalla, E.; Klein, D. R.; Cheng, R.; Seyler, K. L.; Zhong, D.; Schmidgall, E.; McGuire, M. A.; Cobden, D. H.; Yao, W.; Xiao, D.; Jarillo-Herrero, P.; Xu, X. D., Layer-dependent ferromagnetism in a van der Waals crystal down to the monolayer limit. *Nature* **2017**, *546* (7657), 270-273.
- (40) Wang, C.; Zhou, X. Y.; Zhou, L. W.; Pan, Y. H.; Lu, Z. Y.; Wan, X. G.; Wang, X. Q.; Ji, W., Bethe-Slater-curve-like behavior and interlayer spin-exchange coupling mechanisms in two-dimensional magnetic bilayers. *Phys. Rev. B* **2020**, *102* (2), 020402.
- (41) Cardias, R.; Szilva, A.; Bergman, A.; Di Marco, I.; Katsnelson, M. I.; Lichtenstein, A. I.; Nordstrom, L.; Klautau, A. B.; Eriksson, O.; Kvashnin, Y. O., The Bethe-Slater curve revisited; new insights from electronic structure theory. *Sci. Rep.* **2017**, *7*, 4058.
- (42) Yazyev, O. V., Emergence of magnetism in graphene materials and nanostructures. *Rep. Prog. Phys.* **2010**, *73* (5), 056501.
- (43) Liu, J. P.; Ma, Z.; Gao, J. H.; Dai, X., Quantum valley hall effect, orbital magnetism, and anomalous hall effect in twisted multilayer graphene systems. *Phys. Rev. X* **2019**, *9* (3), 031021.
- (44) Sharpe, A. L.; Fox, E. J.; Barnard, A. W.; Finney, J.; Watanabe, K.; Taniguchi, T.; Kastner, M. A.; Goldhaber-Gordon, D., Emergent ferromagnetism near three-quarters filling in twisted bilayer graphene. *Science* **2019**, *365* (6453), 605-608.
- (45) Bultinck, N.; Chatterjee, S.; Zaletel, M. P., Mechanism for anomalous hall ferromagnetism in

- twisted bilayer graphene. Phys. Rev. Lett. 2020, 124 (16), 166601.
- (46) Cao, Y.; Rodan-Legrain, D.; Rubies-Bigorda, O.; Park, J. M.; Watanabe, K.; Taniguchi, T.; Jarillo-Herrero, P., Tunable correlated states and spin-polarized phases in twisted bilayer-bilayer graphene. *Nature* **2020**, *583* (7815), 215-220.
- (47) Chen, G. R.; Sharpe, A. L.; Fox, E. J.; Zhang, Y. H.; Wang, S. X.; Jiang, L. L.; Lyu, B.; Li, H. Y.; Watanabe, K. J.; Taniguchi, T.; Shi, Z. W.; Senthil, T.; Goldhaber-Gordon, D.; Zhang, Y. B.; Wang, F., Tunable correlated chern insulator and ferromagnetism in a moire superlattice. *Nature* **2020**, *579* (7797), 56-61.
- (48) Li, J. C.; Sanz, S.; Castro-Esteban, J.; Vilas-Varela, M.; Friedrich, N.; Frederiksen, T.; Pena, D.; Pascual, J. I., Uncovering the triplet ground state of triangular graphene nanoflakes engineered with atomic precision on a metal surface. *Phys. Rev. Lett.* **2020**, *124* (17), 177201.
- (49) Mishra, S.; Beyer, D.; Eimre, K.; Kezilebieke, S.; Berger, R.; Groning, O.; Pignedoli, C. A.; Mullen, K.; Liljeroth, P.; Ruffieux, P.; Feng, X. L.; Fasel, R., Topological frustration induces unconventional magnetism in a nanographene. *Nature Nanotech.* **2020**, *15* (1), 22-28.
- (50) Mishra, S.; Beyer, D.; Eimre, K.; Ortiz, R.; Fernandez-Rossier, J.; Berger, R.; Groning, O.; Pignedoli, C. A.; Fasel, R.; Feng, X. L.; Ruffieux, P., Collective all-carbon magnetism in triangulene dimers. *Angew. Chem. Int. Ed.* **2020**, *59* (29), 12041-12047.
- (51) Zheng, Y. Q.; Li, C.; Zhao, Y.; Beyer, D.; Wang, G. Y.; Xu, C. Y.; Yue, X. L.; Chen, Y. P.; Guan, D. D.; Li, Y. Y.; Zheng, H.; Liu, C. H.; Luo, W. D.; Feng, X. L.; Wang, S. Y.; Jia, J. F., Engineering of magnetic coupling in nanographene. *Phys. Rev. Lett.* **2020**, *124* (14), 147206.
- (52) Fang, H.; Masaki, M.; B, A.; Puthirath; M, J.; Moya; Gao, G.; Morosan, E.; Ajayan, P. M.; Therrien, J.; Jena, P., U-carbon: Metallic and magnetic. *arXiv* **2020**, 2008.01137.

- (53) Kresse, G.; Furthmüller, J., Efficiency of ab-initio total energy calculations for metals and semiconductors using a plane-wave basis set. *Comput. Mater. Sci.* **1996**, *6* (1), 15-50.
- (54) Blöchl, P. E., Projector augmented-wave method. *Phys. Rev. B* **1994**, *50* (24), 17953-17979.
- (55) Perdew, J. P.; Burke, K.; Ernzerhof, M., Generalized gradient approximation made simple. *Phys. Rev. Lett.* **1996,** 77 (18), 3865-3868.
- (56) Perdew, J. P.; Chevary, J. A.; Vosko, S. H.; Jackson, K. A.; Pederson, M. R.; Singh, D. J.; Fiolhais, C., Atoms, molecules, solids, and surfaces: Applications of the generalized gradient approximation for exchange and correlation. *Phys. Rev. B* **1992**, *46* (11), 6671-6687.
- (57) Monkhorst, H. J.; Pack, J. D., Special points for brillouin-zone integrations. *Phys. Rev. B* **1976**, 13 (12), 5188-5192.
- (58) Togo, A.; Tanaka, I., First principles phonon calculations in materials science. *Scripta Mater.* **2015,** *108*, 1-5.
- (59) Galeev, T. R.; Dunnington, B. D.; Schmidt, J. R.; Boldyrev, A. I., Solid state adaptive natural density partitioning: A tool for deciphering multi-center bonding in periodic systems. *Phys. Chem. Chem. Phys.* **2013**, *15* (14), 5022-5029.
- (60) Zubarev, D. Y.; Boldyrev, A. I., Developing paradigms of chemical bonding: Adaptive natural density partitioning. *Phys. Chem. Chem. Phys.* **2008**, *10* (34), 5207-5217.
- (61) Dunnington, B. D.; Schmidt, J. R., Generalization of natural bond orbital analysis to periodic systems: Applications to solids and surfaces via plane-wave density functional theory. *J. Chem. Theory Comput.* **2012**, *8* (6), 1902-1911.
- (62) Fujimori, M.; Nakata, T.; Nakayama, T.; Nishibori, E.; Kimura, K.; Takata, M.; Sakata, M., Peculiar covalent bonds in α-rhombohedral boron. *Phys. Rev. Lett.* **1999**, *82* (22), 4452-4455.

## Figure captions:

Figure 1. Side view of α-boron in hexagonal representation (a). The solid lines with red, blue, and pink colors indicate the corresponding (001), (10-2), and (101) planes of α-boron. Side view and top view of face-boron, t-face-boron, and edge-boron (b-d), which are cleaved from α-boron along the (001), (10-2), and (101) planes, respectively. The boron atoms in the outermost surface of face-boron, t-face-boron, and edge-boron with unsaturated bonds are depicted in red, blue, and pink colors, respectively. The other boron atoms that also have unsaturated bonds in t-face-boron and edge-boron are depicted in cyan color. Within each of these structures the bonds within the boron icosahedra can be classified as 3c-2e bonds. The icosahedra surrounded by six icosahedra with six 3c-2e bonds in face-boron are represented by green triangles. The icosahedra in t-face-boron and edge-boron are connected by 2c-2e bonds. The three exchange coupling paths inside each icosahedron (XC<sub>intra-i</sub>) and between the icosahedra (XC<sub>intra-b</sub>) in the surface, and those between the upper and lower surfaces (XC<sub>intra</sub>) are indicated by black solid two-way arrows.

Figure 2. Band structures in a fat-band representation and LDOS of face-boron, t-face-boron, and NM edge-boron (a-c). The Fermi level is presented by the horizontal dashed line.

Figure 3. Spin-polarized band structure, DOS, and charge density using an isosurface level of 0.005 eV/A<sup>3</sup> of AFM-4 edge-boron (a-b) and 2-layer AFM-1 edge-boron (c-d). The yellow color represents electron spin up and the cyan color represents spin down.

Figure 4. Relationship between the band gaps calculated using GGA-PBE and number of layers (n) in the unit cell of face-boron, t-face-boron, and edge-boron in their ground states (a). The cyan solid line indicates the band gap of bulk  $\alpha$ -boron. It is noted that the energy bands of the upper and lower surfaces of edge-boron are not completely degenerate at 3~4 layers. The relationship between the

energy difference ( $E_d$ ) and n of edge-boron (b). The total energy of NM edge-boron is used as the reference. The energy differences between the most stable AFM and FM configurations as a function of n of edge-boron (c). The spacing of edge-boron corresponding to n are shown in the top axis. The total energy of 1-layer NM edge-boron is used as a reference at n = 1 because geometrical relaxation of the FM configurations converged to a NM configuration.

FIG. 1.

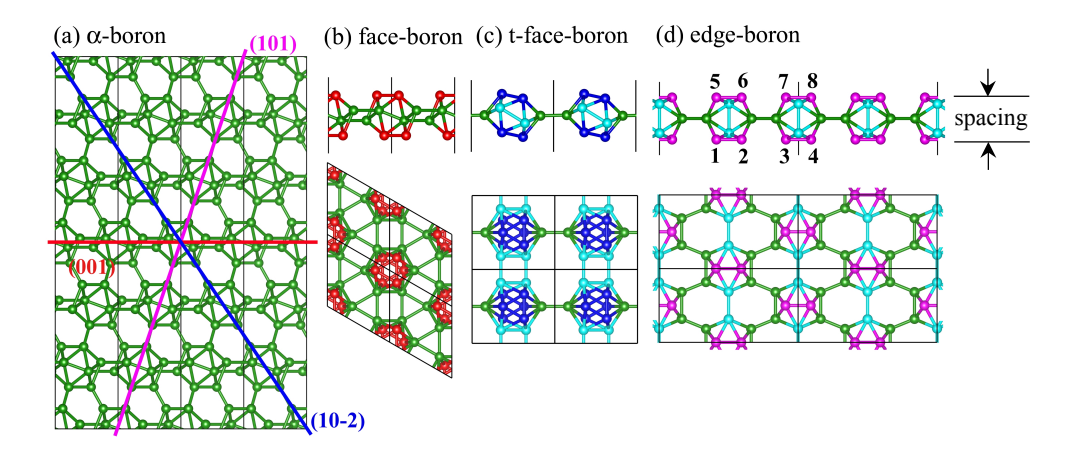
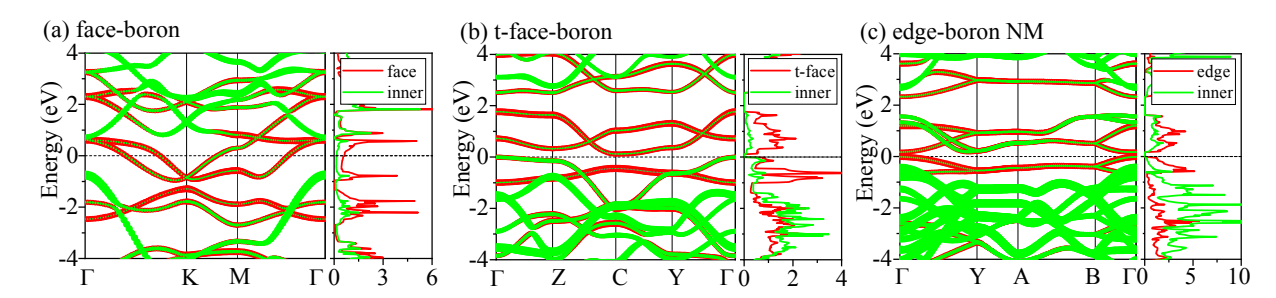


FIG. 2.



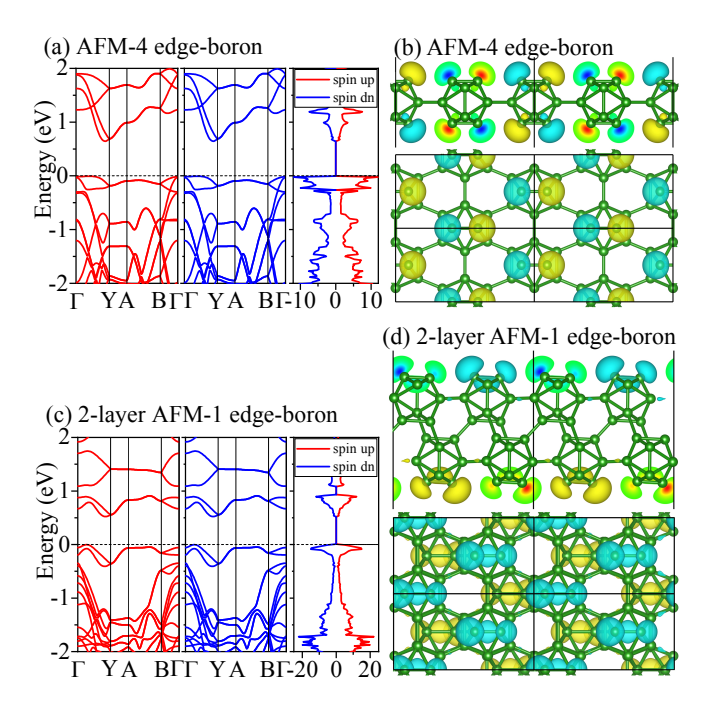


FIG. 4.

